Clays and Clay Minerals, Vol. 47, No. 3, 269–285, 1999.

CLAY DIAGENESIS IN THE SANDSTONE RESERVOIR OF THE ELLON FIELD (ALWYN, NORTH SEA)

LHOUSSAIN HASSOUTA, MARTINE D. BUATIER, JEAN-LUC POTDEVIN, AND NICOLE LIEWIG[1]

Université Lille 1, URA 719, Laboratoire de Sédimentologie et Géodynamique, 59655 Villeneuve d'Ascq, France
[1] Centre de Géochimie de la Surface, CNRS, 1, rue Blessig, 67084 Strasbourg Cedex, France

Abstract—The nature, composition, and relative abundance of clay minerals in the sandstones of the Brent Group reservoir were studied between 3200–3300 m in a well of the Ellon Field (Alwyn area, North Sea). The sandstones have a heterogeneous calcite cement which occurred during early-diagenesis. Clay diagenesis of the cemented and uncemented sandstones was investigated using optical microscopy, scanning electron microscopy (SEM), X-ray diffraction analyses (XRD), and infrared spectroscopy (IR). The influence of cementation on clay neoformation is demonstrated in this study. Detrital illite and authigenic kaolinite are present in both the calcite-cemented and uncemented sandstones suggesting that kaolinite precipitated before calcite cementation. In the uncemented sandstones, blocky dickite replaces vermiform kaolinite with increasing depth. At 3205 m, authigenic illite begins to replace kaolinite and shows progressive morphological changes (fibrous to lath-shape transition). At 3260 m, all sandstones are not cemented by calcite. Illite is the only clay mineral and shows a platelet morphology.

In the cemented samples, vermiform kaolinite is preserved at all depths, suggesting that dickite transformation was inhibited by the presence of the calcite cement. This observation suggests that calcite cement would prevent fluid circulation and dissolution-precipitation reactions.

Key Words—Calcite, Diagenesis, Dickite, Illite, Kaolinite, North Sea, Pressure-Solution, Sandstone.

INTRODUCTION

Clay diagenesis can greatly change the physical properties of sandstones in petroleum reservoirs. Precipitation of clay minerals in the pore spaces and the evolution of clays through burial and temperature were described by many authors; for instance, in the Brent Group reservoirs of the (Middle Jurassic) North Sea, the evolution of illite and kaolin morphologies with depth and temperature is well documented (Kantorowicz, 1984; Thomas, 1986; Glasmann *et al.*, 1989; Giles *et al.*, 1992; Haszeldine *et al.*, 1992). Ehrenberg *et al.* (1993) and Lanson *et al.* (1996) showed the relationship between kaolin morphology (*i.e.*, vermicular or blocky kaolin) and the nature of the kaolin polytype (*i.e.*, kaolinite or dickite). In the Brent Group reservoirs, illite replaces kaolinite and muscovite and shows morphological changes with burial depth. The illitization of kaolinite was described by Bjørlykke (1983) by the reaction: Kaolinite + K-feldspar → Illite + Quartz. According to Ehrenberg *et al.* (1993) and Lanson *et al.* (1996), the kaolin-polytype evolution and the illitization reaction are temperature dependant. The purpose of this paper is to describe clay diagenesis in a sandstone reservoir of the Brent Group in the North Sea that is heterogeneously cemented by calcite. We compare clay diagenesis in early calcite-cemented sandstones with sandstones in which the calcite cement was absent during burial diagenesis. These comparisons allow discussion of the mechanisms of illite precipitation and the kaolinite to dickite transition with reference to depth, lithology, and cementation.

GEOLOGICAL SETTING

The studied sandstones were collected from a well of the Ellon Field (North Sea), located in the Great Alwyn area (Figure 1). The Alwyn area is a intermediate-faulted terrace between the East Shetland Platform and the Viking Graben. The structure of the Ellon Field is mainly the result of rifting of the Viking Graben in two stages (Faure, 1990). The first stage occurred from Permian to Triassic. The second stage is Jurassic and resulted in tilted block faulting. Then, an important erosion and a meteoric fluid flow episode occurred during the Cimmerian phase (Sommer, 1978). A new stage of tectonic extension occurred during the late Cretaceous with a high sedimentation rate which sealed the basin structure. The studied sandstones belong to the Brent Group which contains the most prolific petroleum reservoirs in the northern North Sea Basin (Blanche and Whitaker, 1978, Hancock and Taylor, 1978, Giles *et al.*, 1992). The Brent Group is composed of five Jurassic formations (late Bajocian to early Bathonian): Broom, Rannoch, Etive, Ness, and Tarbert (Bowen, 1975; Deegan and Scull, 1977). From a sedimentological view, the Brent sequence records the progression from the coastal shallow-marine environments of the Lower Brent Group, to the alluvial or deltaic interbedded sands, shales, and coals of the Middle Brent, and ends with the transitional to marine sands of the Upper Brent Group (Jourdan *et al.*, 1987). In the studied well, only the Ness B and Tarbert Formations were cored (Figure 2). The Ness B is divided into a lower tide-dominated section and an upper section of three shoreface-tidal complexes. These two

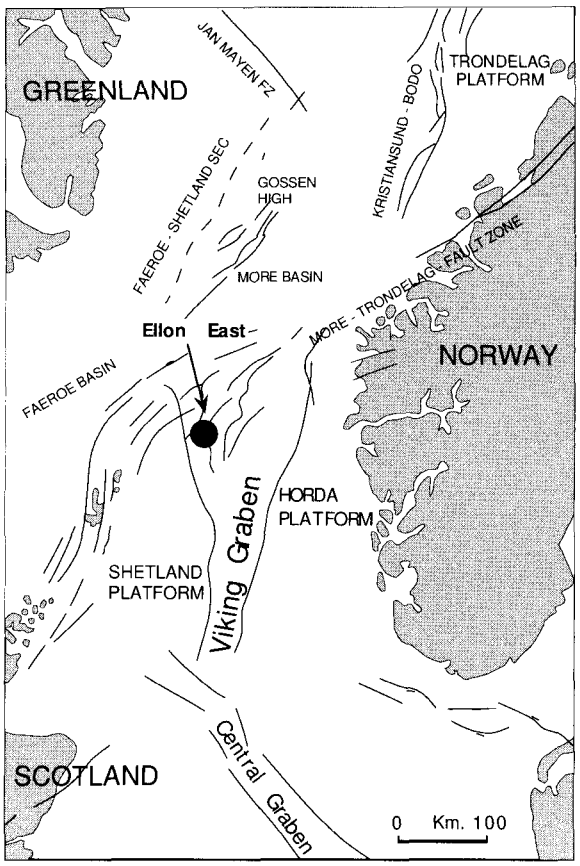

Figure 1. Location map of the studied well.

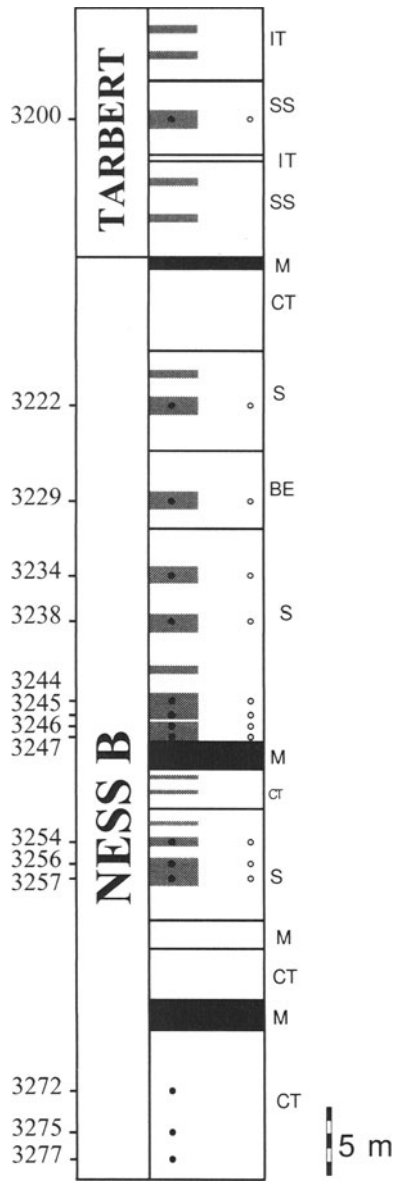

Figure 2. Schematic log of the sedimentary facies within the studied well. Symbols: IT = Transgressive lag, SS = Upper shoreface, M = Marsh, S = Shoreface, CT = Tidal complex, BE = Mouth bar. Coal and organic shale are in black. The cemented zones are shown in grey. The filled circles are cemented samples. The open circles represent uncemented samples.

parts are separated by thin lagoonal or coaly-marsh facies. The lower Tarbert Formation comprises two upper shorefaces separated by a thin transgressive lag. The upper Tarbert Formation consists of a thick transgressive lag (Figure 2). The sandstones from the Ness and Tarbert formations are heterogeneously cemented by calcite from 3200 to 3260 m. Below 3260 m, the calcite cement is absent.

SAMPLING APPROACH

Sampling has focused on comparison of calcite-cemented sandstones and sandstones where the calcite cement is absent ("uncemented" sandstones). Both sandstones were sampled at different depths in the Ness and Tarbert Formations of the Brent Group (Figure 2; Table 1). Calculated and measured porosities of the studied sandstones are ~20% in the uncemented sandstones and <3% in the cemented sandstones (Potdevin and Hassouta, 1997). Considering the calcite content of the cemented sandstones, the initial porosity before cementation was ~40%. This high initial porosity and the sparitic texture of the cement suggest that calcite cementation was an early diagenetic process occurring at shallow depth, as suggested by Ziegler and Spotts (1978). The calcite cementation is heterogeneous. The contact between cemented and uncemented sandstones is always very sharp (Figure 3) and does not seem to correspond to an initial heterogeneity but may be a dissolution or a precipitation front. The early calcite cementation and the very low porosity of the cemented sandstones preserved the sandstone grains from water-rock interactions and fluid flow during burial. Studying the cemented and unce-

https://doi.org/10.1346/CCMN.1999.0470303 Published online by Cambridge University Press

Table 1. Summary of major physical properties of the studied samples.

Sample depth (m) TVD	Formation	Facies	Calcite cement	Medium grain size (μm)	Sorting	Optical porosity
3200 nc	TARBERT	SS	—	—	—	24
3200 c	TARBERT	SS	X	—	—	—
3222 nc	NESS	S	—	—	—	20
3222 c	NESS	S	X	—	—	—
3229 nc	NESS	BE	—	180	PM	22
3229 c	NESS	BE	X	—	—	—
3234 nc	NESS	S	—	—	—	15
3234 c	NESS	S	X	—	—	—
3238 nc	NESS	S	—	155	W	20
3238 c	NESS	S	X	160	W	—
3244 nc	NESS	S	—	170	W	22
3244 c	NESS	S	X	162	W	—
3245 nc	NESS	S	—	145	W	20
3245 c	NESS	S	X	142	W	—
3246 nc	NESS	S	—	130	W	16
3246 c	NESS	S	X	—	—	—
3254 nc	NESS	S	—	155	W	17
3254 c	NESS	S	X	160	W	—
3256 nc	NESS	S	—	160	W	15
3256 c	NESS	S	X	150	W	—
3257 nc	NESS	S	—	—	—	13
3257 c	NESS	S	X	—	—	—
3272	NESS	CT	—	—	—	19
3275	NESS	CT	—	185	W	12
3277	NESS	CT	—	—	—	16

X = present, SS = Upper shoreface, S = Shoreface, BE = Mouth bar, CT = Tidal complex, PM = poor to moderate, W = well, nc = uncemented sandstone, c = cemented sandstone.

mented sandstones allows us to compare clay burial diagenesis in water-present and water-absent sandstones of the same initial composition. Twenty four pairs of adjacent cemented and uncemented sandstones were sampled to compare clay diagenesis as a function of depth, lithology, and cementation (Table 1).

METHODS AND ANALYTICAL TECHNIQUES

Thin sections were examined using petrographic and cathodoluminescence microscopes. A Technosyn Cold Cathodoluminescence Model 8200 MkII operating at 15–20 kv and 350 μA was used. Bulk samples were also observed by scanning electron microscopy (SEM) at 15 kv with a Cambridge Stereoscan 240. Samples located in the oil zone were washed at the Total-Beauplan Centre to remove organic matter (hydrocarbons) from the pore spaces. The clay size fractions (<2 μm and <5 μm) were separated from bulk samples by settling in a water column. Prior to separation, each sample was dispersed in deionized water, disaggregated and decarbonated with a 0.2 M HCl solution and washed several times. Clay mineral assemblages were determined by X-ray diffraction (XRD) on oriented and powdered samples with a Philips PW 1729 diffractometer using CuKα radiation and a Ni filter with a scan speed of 2 °2θ/min. The modeling

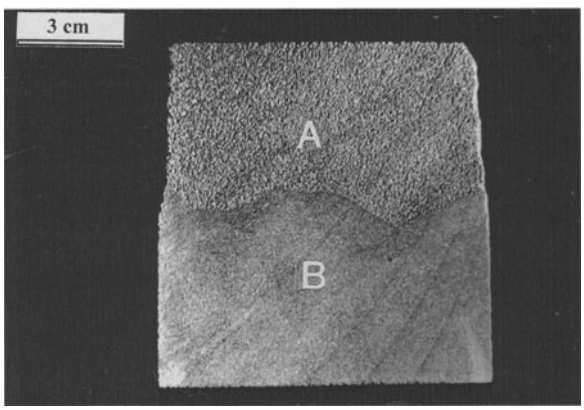

Figure 3. Section of sample (3244) showing the sharp transition between (A) uncemented sandstone and (B) a calcite cemented sandstone.

program of Lanson and Besson (1992) was used to analyze XRD patterns of clay minerals in the range 5–12.5 °2θ. This program allows the determination of the composition of the clay mineral fraction by fitting the XRD pattern to the sum of the theoretical individual patterns of different clay minerals. Infrared spectra were recorded in the 3800–200 cm^{-1} range on a Nicollet 510 infrared spectrophotometer using pressed disks prepared by mixing 4 mg of sample with 300 mg of KBr. Chemical analyses of selected minerals were performed using the electron microprobe Camebax, SX 50 model, of the Camparis Center of Paris VII University. Standards were natural silicates and oxides, the accelerating voltage was 15 kv, the counting time 10–20 s, the current intensity 15 nA and the spot size 1 μm.

RESULTS

Petrography

The bulk mineralogy is very similar in all sandstones (Table 2). The detrital grains are quartz, feldspars (albite and microcline), mica, and various types of lithic fragments. Mineralogic variations concern principally the diagenetic phases which are calcite cement, quartz overgrowth, pyrite, kaolin, and illite. Minor ankerite was also detected by XRD. Calcite and ankerite are only present in cemented sandstones and are absent below 3260 meters. Kaolin minerals occur in cemented and uncemented sandstones above 3260 m. Quartz overgrowths and illite are very rare in cemented sandstones but abundant in uncemented sandstones located below 3205 m.

Quartz. Quartz represents 50–70% of the sandstones. It is mostly detrital but quartz overgrowths are common in the uncemented sandstones. The detrital core is rimmed by one or two stages of diagenetic quartz, reducing the pore space between grains. Overgrowths give an euhedral shape to quartz grains as shown on

https://doi.org/10.1346/CCMN.1999.0470303 Published online by Cambridge University Press

Table 2. Mineralogical data on the studied samples. Relative abundances of each mineral were calculated from modal analyses calculated from point counting on thin section. XRD data are also presented in this table.

Sample depth (m) TVD	Cal	Rf	Om	Py	Q	K-F	Ab	M	Qo	ill	Kln	K[1]	D[1]	ill[1]
3200 nc	0.0	0.0	0.8	0.4	65.6	4.4	0.0	0.2	3.2	0.2	0.6	XX	—	—
3200 c	40.0	0.6	0.0	0.0	55.2	4.2	0.0	0.0	—	0.0	0.0	XX	—	—
3222 nc	0.0	0.4	2.5	0.7	57.3	3.6	0.2	2.0	6.8	3.6	2.2	XX	—	X
3222 c	42.9	1.7	5.3	0.6	39.2	3.8	0.3	4.1	—	0.0	1.9	XX	—	—
3229 nc	0.0	0.1	1.8	0.0	51.8	3.2	0.2	1.7	6.0	6.3	6.0	XX	—	X
3229 c	47.9	0.5	0.0	1.9	41.1	4.0	0.8	0.7	—	0.4	2.7	XX	—	—
3234 nc	0.0	0.4	5.4	1.5	49.8	3.6	0.8	5.1	6.4	6.7	5.3	XX	X	X
3234 c	43.3	1.3	4.5	1.5	40.2	4.2	0.1	3.2	—	0.0	1.7	XX	—	—
3238 nc	0.0	2.5	0.0	2.9	54.9	2.5	0.2	4.1	3.8	5.1	3.8	XX	X	X
3238 c	42.3	3.6	0.0	3.7	38.1	5.3	0.0	3.2	—	0.9	2.8	XX	—	—
3244 nc	0.0	0.6	2.0	1.1	55.5	1.5	0.5	3.7	4.2	4.8	3.8	XX	X	X
3244 c	47.4	1.0	3.2	1.2	40.6	2.2	0.4	2.2	—	0.8	1.0	XX	—	—
3245 nc	0.0	1.2	3.5	1.6	52.1	2.9	0.2	3.3	3.7	6.2	4.6	X	X	X
3245 c	43.6	0.0	3.4	1.6	42.8	3.0	0.0	3.0	—	0.0	2.6	XX	—	—
3246 nc	0.0	1.2	2.6	1.0	49.4	2.2	0.4	4.2	8.5	7.8	6.2	X	X	X
3246 c	46.5	1.0	2.1	0.5	43.4	2.6	0.0	2.6	—	0.0	1.3	XX	—	—
3254 nc	0.0	1.8	2.0	2.2	47.1	2.6	0.0	5.0	6.6	11.1	4.2	X	XX	X
3254 c	45.0	6.6	0.0	2.8	39.6	2.2	0.0	2.8	—	0.0	1.0	XX	—	—
3256 nc	0.0	0.5	2.4	2.2	51.4	2.5	0.2	5.0	5.2	11.1	4.5	—	XX	X
3256 c	49.1	0.7	1.9	5.1	36.5	2.8	0.2	1.9	—	0.9	0.9	XX	—	—
3257 nc	0.0	1.6	2.9	5.5	50.4	2.8	0.4	6.3	4.9	8.7	2.9	—	XX	XX
3257 c	46.4	1.0	2.3	4.9	37.0	2.5	0.2	4.2	—	0.2	1.3	XX	—	—
3272	0.0	2.8	0.0	1.7	63.5	0.3	0.0	4.8	3.0	4.9	0.0	—	—	XX
3275	0.0	2.0	0.2	2.6	67.8	1.6	0.0	2.8	4.6	6.2	0.0	—	—	XX
3277	0.0	0.6	1.8	2.6	70.8	1.0	0.0	2.0	2.4	2.8	0.0	—	—	XX

[1] Data from XRD, X = present, XX = dominant.

Cal = Calcite, Rf = Rock fragments, Om = Organic matter, Py = Pyrite, Q = Quartz, K-F = K-Feldspar, Ab = Albite, M = Mica, Qo = Quartz Overgrowths, ill = illite, Kln = Kaolin, K[1] = Kaolinite; D[1] = Dickite, ill[1] = illite, nc = uncemented sandstone, c = cemented sandstone.

optical microscope images (Figure 4A). Indented and stylolitized contacts between quartz grains indicate that pressure-solution was an efficient mechanism decreasing rock porosity. Quartz overgrowths are absent in the calcite cemented sandstones.

Feldspar. K-feldspar is the most abundant feldspar but its concentration depends on the sedimentary facies. According to modal analyses, K-feldspar represents 4–5% of the rock volume in the upper shoreface but 1–7% in the lower shoreface facies. The amount of K-feldspar also varies with increasing depth and cementation. When depth increases, most feldspars display dissolution marks in uncemented sandstones (Figure 4B). In calcite-cemented sandstones, K-feldspars are well preserved (Figure 4C) and can display an euhedral shape which results in thin K-felspar overgrowths. The microprobe analyses show a very pure K-feldspar composition of these overgrowths. They are black (nonluminescent) in cathodoluminescence, indicating a very low trace-element content resulting from a low temperature of crystallization (*i.e.*, <100°C, Marshall, 1988); this confirms their authigenic origin. K-feldspar overgrowths are not observed in uncemented sandstones. The lack of overgrowths could result in an important dissolution of the K-feldspar grains in these sandstones.

Detrital mica. Detrital muscovite is present in all samples. The amount is not related to cementation, but it is dependant on the sedimentary facies. Undulatory extinction and flexed mica crystals in the uncemented sandstones suggest that deformation occurred during compaction. In calcite-cemented sandstones, mica grains are well preserved with minor kaolinitization developed only at the grain boundaries (Figure 4D), whereas in uncemented sandstones the micas display open layers filled by kaolin and illite. In some crystals, these two minerals entirely replace the mica.

Calcite. In cemented sandstones, a calcite cement fills the pores. The calcite occurs as large crystals in which detrital grains are enclosed. Despite evidence of intense recrystallization, cathodoluminescence reveals growth zones which show the sparitic nature of the early cement. The microprobe analyses show that the calcite crystals have the structural formula: $Ca_{0.948}Mg_{0.047}Mn_{0.004}Sr_{0.001}Ba_{0.001}CO_3$. Some relics of the calcite cement were found inside quartz overgrowths suggesting a dissolution episode of the calcite cement prior to quartz cementation.

Kaolin minerals. Three morphologies of kaolin minerals were observed by SEM. (1) Vermiform kaolin

https://doi.org/10.1346/CCMN.1999.0470303 Published online by Cambridge University Press

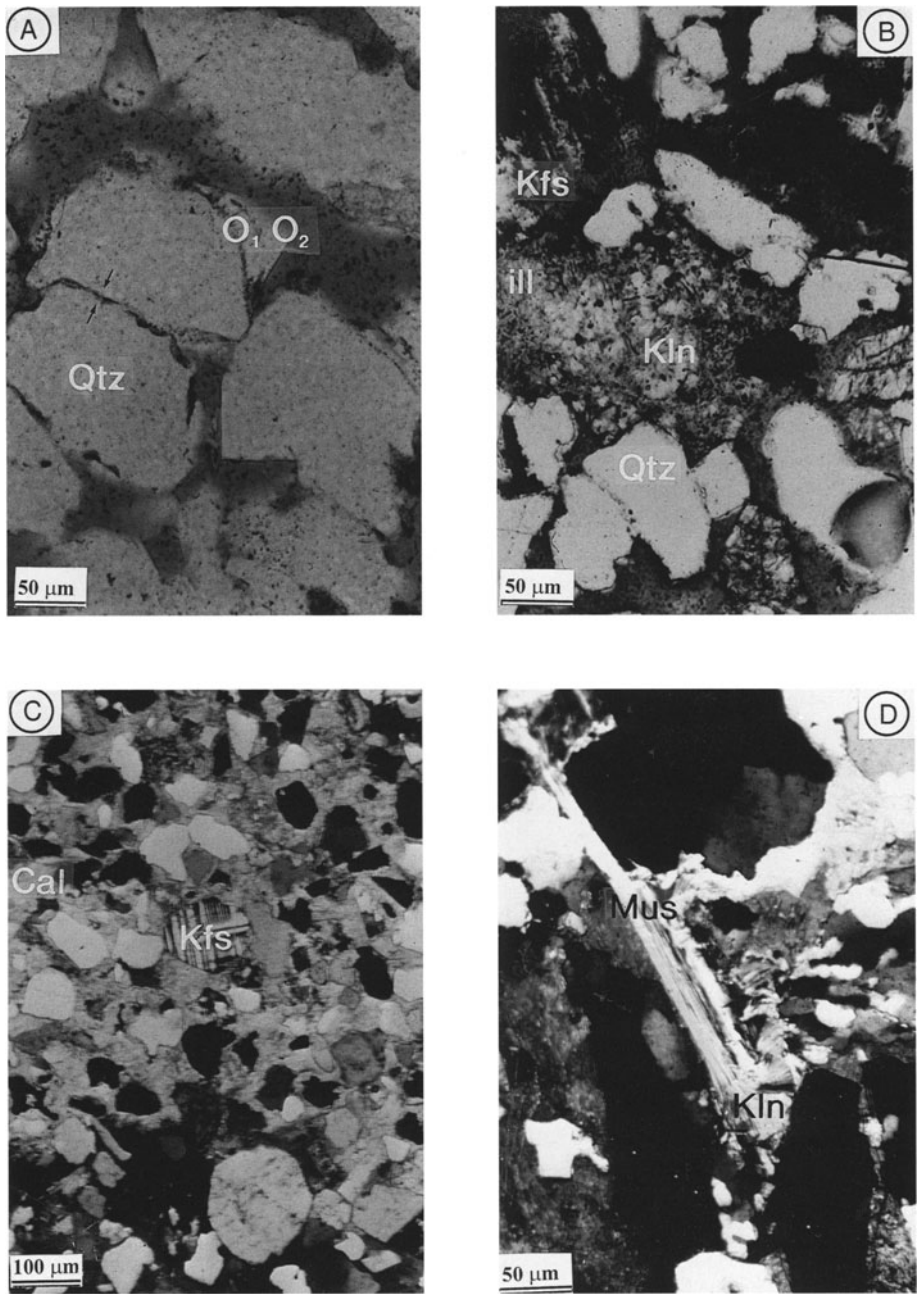

Figure 4. Optical microscope image of studied sandstones. (A) Quartz grains showing one or two phases of overgrowth (O1 and O2), indented contacts between detrital grains of quartz are shown by arrows, (B) dissolved K-feldspar in uncemented sandstone, (C) preserved microcline (Kfs) in cemented sandstone, and (D) alteration of muscovite to kaolinite in a cemented sandstone. The kaolinite crystals appear at the edge of the muscovite crystal. Plane polarized light. Symbols: Qtz = Quartz, Kfs = K-Feldspar, Mus = Muscovite, Kln = Kaolinite, ill = illite, Cal = Calcite.

fills the pores (Figure 5A). (2) Cluster kaolin (Figure 5B) forms adjacent to, or between, expanded layers of detrital mica. This morphology is common in the Ness Formation, particularly in the shoreface facies, and is probably the result of the higher concentration of muscovite in these sandstones. Vermiform and cluster morphologies are present both in cemented and uncemented sandstones suggesting that kaolinite precipitation preceded calcite cementation. (3) Blocky kaolin (Figure 5C) is present in the deeper uncemented samples (≥3232 m) but absent in the corresponding cemented sandstones and very rare in impermeable coaly-marsh facies. These crystals are pseudo-hexagonal in shape, 5–10 μm in thickness with a diameter of 10–

https://doi.org/10.1346/CCMN.1999.0470303 Published online by Cambridge University Press

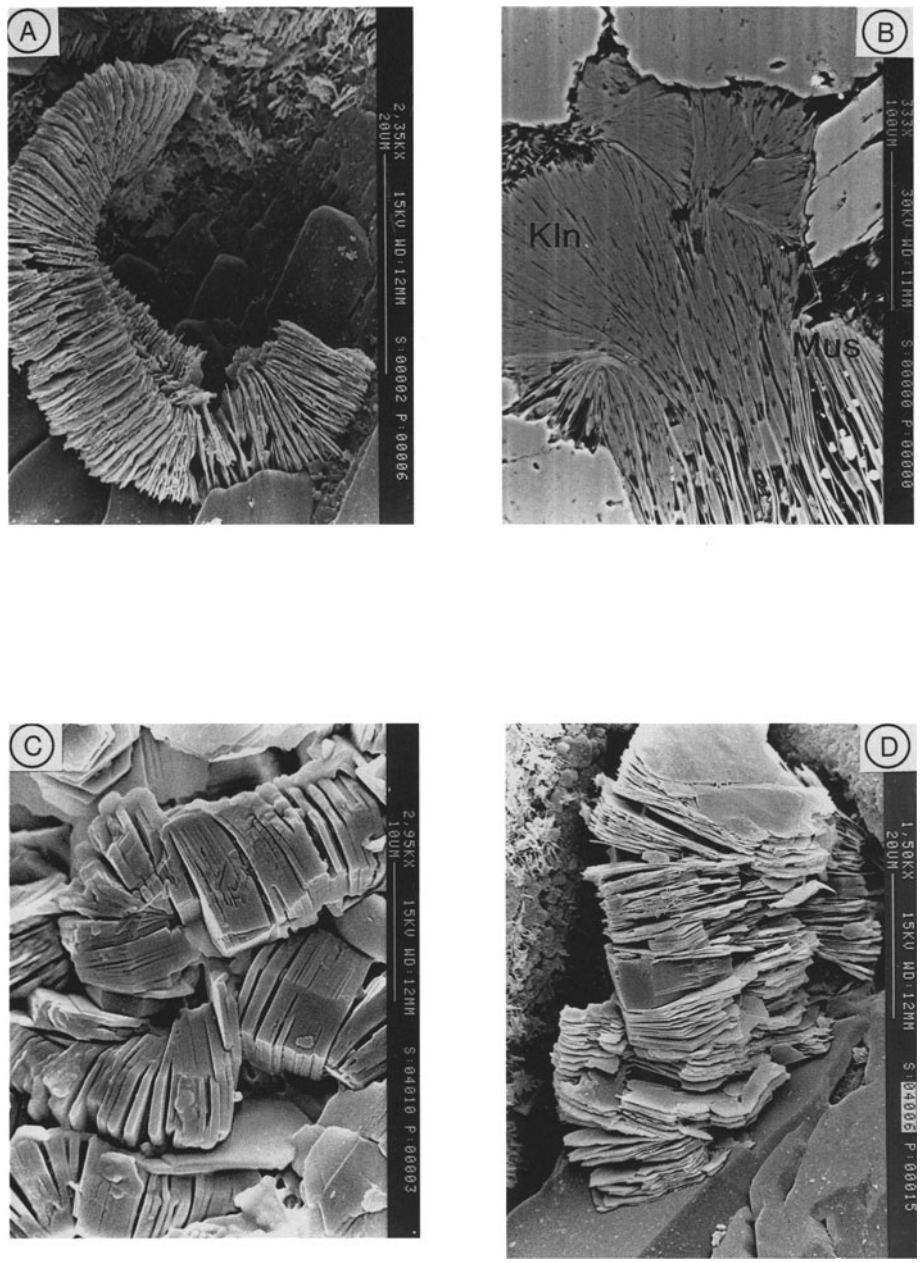

Figure 5. SEM micrographs of the kaolin polytype morphologies. (A) Vermiform kaolin crystals (3204 m), (B) Cluster kaolin crystals (3224 m), (C) Blocky kaolin crystals (3254 m), (D) Replacement of vermiform kaolin by blocky crystals (3204 m). (A), (C), and (D) are secondary electron images. (B) is a backscattered electron image. Symbols: Mus = Muscovite, Kln = Kaolinite.

20 μm. This morphology is absent in all calcite-cemented sandstones.

SEM observations of the kaolin morphologies in the uncemented sandstones show a progressive change with depth. In the most shallow samples (3200 m), aggregates of vermiform kaolin crystals were observed, ~80–100 μm, and the diameter of the vermicules is <10 μm. Deeper in the core (~3204 m), the vermiform crystals are progressively replaced by larger crystals (diameter >10 μm) (Figure 5D). Between 3254-3260 m, the blocky morphology is dominant. In the cemented sandstones, only vermiform and cluster kaolinite crystals are observed. Below 3260 m, no kaolin was observed by SEM.

Diagenetic illite. Diagenetic illite is only present in the uncemented sandstones. It occurs as aggregates of small crystals filling the pore spaces. Illite can replace

https://doi.org/10.1346/CCMN.1999.0470303 Published online by Cambridge University Press

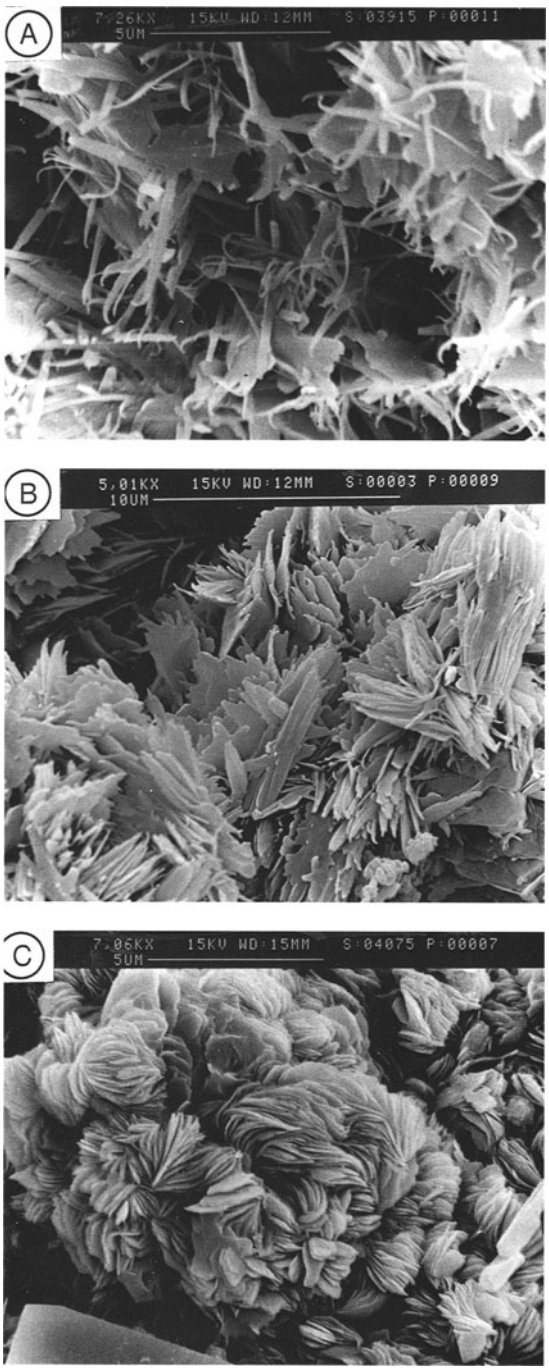

Figure 6. SEM micrographs of illite morphology changes with depth. (A) Filamentous illite (3204 m), (B) lath illite (3244 m), (C) platelet illite (>3260 m).

the kaolin minerals and detrital muscovite. In SEM images, kaolinite aggregates are replaced by fibrous illite. The SEM images show that illite morphology varies with depth. Filamentous illite (Figure 6A) is observed in the shallowest samples (3204 m), and it is followed by lath morphology (3238 m) (Figure 6B). Both morphologies occur with kaolin minerals to a depth of 3260 m. Deeper, illite is the only clay mineral identified. It appears as platelet crystals (Figure 6C) which fill the pores and replace detrital mica.

Clay mineralogy (XRD)

The clay fraction (<5 μm) consists mainly of illite and kaolin (Figure 7). Chlorite is rare and is absent in the upper part of the Tarbert Formation. Kaolins are characterized by the (001) and (002) reflections, respectively, at 7.14 or 7.22 and 3.58 Å. Illite is characterized by the presence of three peaks at 10, 5, and 3.3 Å corresponding respectively to the (001), (002), and (003) reflections. In all of the cemented samples, kaolinite is the major phase in the clay fraction, whereas in the uncemented samples, the intensity of the illite peaks increases with depth. Below 3260 meters, illite is the only clay present in the clay fraction (Table 2).

Kaolin polytype characterization

X-ray diffraction data. The random mounts of the 5-μm fraction of the samples were analyzed to characterize the kaolin polytype present in the sandstones. Polytype identification can be difficult because of the superposition of the quartz and feldspar reflections with those of the kaolin minerals (Ehrenberg *et al.*, 1993). However, some characteristic reflections were used to distinguish the various polytypes. In the cemented samples, kaolinite is the only kaolin polytype and is characterized by reflections at 7.21, 3.58, 3.136, 3.32, and 2.34 Å (Figure 8A). In the uncemented samples, the XRD patterns display mineralogical changes with depth (Figure 9; Table 2). Samples located between 3200–3223 m contain kaolinite. Below 3223 m, the occurrence of a reflection at 4.13 Å indicates the presence of dickite. In samples where dickite is the major kaolin polytype, reflections at 2.32 and 4.13 Å are clearly visible (Figures 8B and 9).

IR spectroscopy. More accurate distinction between kaolinite and dickite can be determined by the position and relative intensity of the OH-stretching bands in the 3600–3700 cm^{-1} region of IR patterns. Well-crystallized kaolinite shows a strong absorption at 3697 cm^{-1}, a band of medium-strong intensity at 3620 cm^{-1} and two bands with relatively weak intensity at 3669 and 3652 cm^{-1}. In contrast, dickite shows a strong absorption band at 3621 cm^{-1} and two medium-strong bands at 3704 and 3654 cm^{-1} (Ehrenberg *et al.*, 1993). IR spectra on the <5-μm fraction of samples from different depths are shown in Figure 10. They confirm the XRD data, *i.e.*, the presence of kaolinite (well-crystallized) in the cemented samples and the presence of dickite in the uncemented samples located at 3254 m (Figure 10A and 10B). The uncemented samples between 3230–3244 m contain both kaolin polytypes. The increase of dickite proportion with depth is clearly

https://doi.org/10.1346/CCMN.1999.0470303 Published online by Cambridge University Press

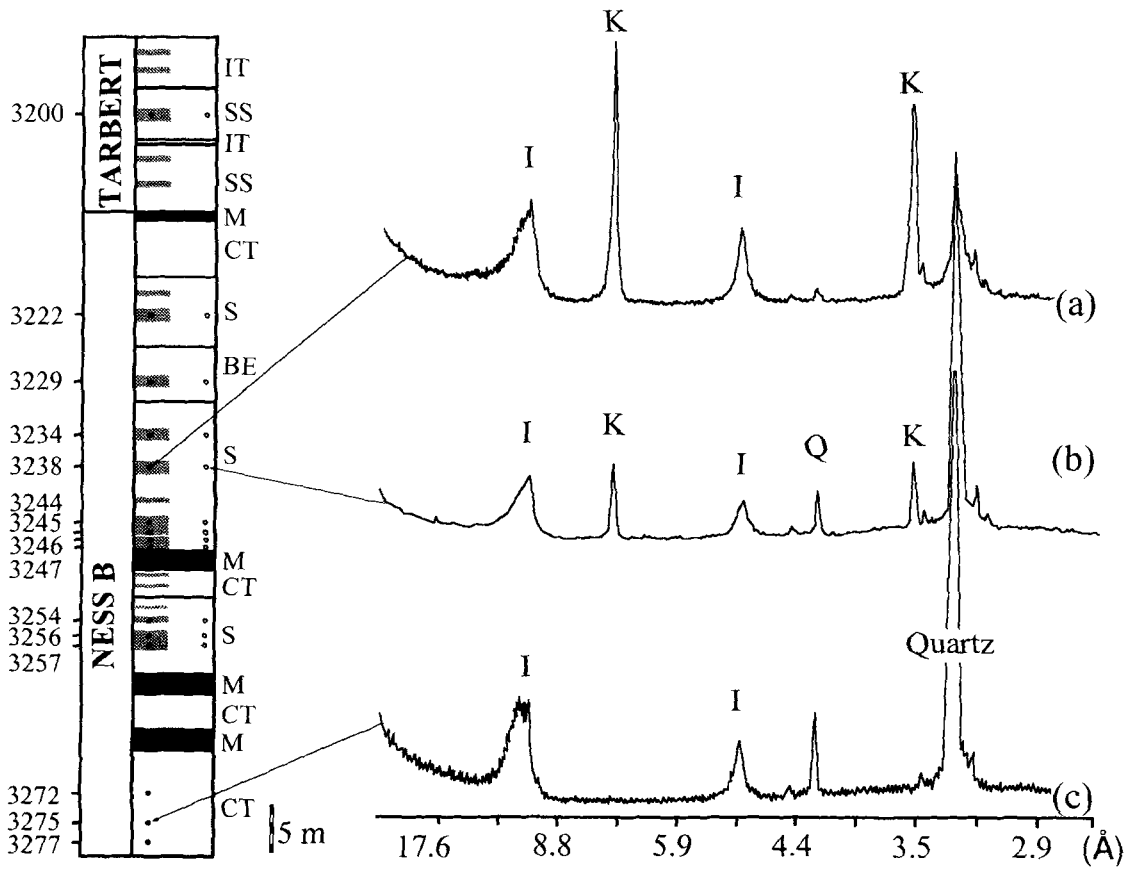

Figure 7. XRD patterns of a pair of cemented (a) and uncemented (b) sandstones from 3238 m. The kaolinite peaks are more intense than illite in the cemented sandstones. (c) XRD patterns of a deep uncemented sandstone (3275 m). The kaolinite peaks are absent.

shown by the IR spectra (Figure 10B). In the sample at 3257 m, a shoulder at 3668 cm^{-1}, characterizing the presence of kaolinite, is still visible in the IR spectra. The higher proportion of kaolinite in this clay fraction could be related to the relatively low porosity of this sample (~13%) compared with the other samples (porosity of ~18%) where kaolinite is in smaller proportion based on IR spectra. In the cemented samples, kaolinite is the only kaolin polytype detected at all depths (<3260 m) (Figure 10A).

Illite characterization

XRD data. The diffraction patterns of the oriented clay fraction of both cemented and uncemented samples display a large and asymmetric peak between 5–11 °2θ (Figure 11). In the air-dried samples located above 3260 m, the most intense peak is at 10 Å; below 3260 m, the illite reflections are the most intense, and a double reflection is visible with a peak at 10.5 Å and another one at 10 Å. After glycolation, the 10.5-Å peak disappears, whereas the peak at 10 Å becomes more intense, but the reflection is asymmetric at the lower °2θ side. A comparison of the XRD data with data generated by the Newmod program (Reynolds, 1985) indicates the presence of illite rich I-S mixed layers (~90% illite layers). With the decomposition method of Lanson and Besson (1992), the simulated XRD pattern reproduces the air-dried experimental pattern in the range 5–11 °2θ when they are generated by three gaussian curves respectively at ~11 (8.03 °2θ), 10.5 (8.5 °2θ), and 10 Å (8.8 °2θ) (Figures 11 and 12). Experimental patterns of the glycolated samples are reproduced correctly with four gaussian curves respectively at ~7.3, 8.3, 8.7, and 8.8 °2θ. These decompositions are very similar to those obtained by Lanson *et al.* (1996) for diagenetic illite from the sandstones of the Rotliegend Formation. According to these authors, these reflections indicate that the illite particles are composed of well crystallized illite (8.8 °2θ in air-dried and glycolated samples), poorly crystallized illite (8.6 °2θ in air-dried samples) and illite-smectite mixed layers with ~80% illite layers (~8 °2θ in air-dried samples). All the samples can be decomposed with similar gaussian-fit curves (*e.g.*,

https://doi.org/10.1346/CCMN.1999.0470303 Published online by Cambridge University Press

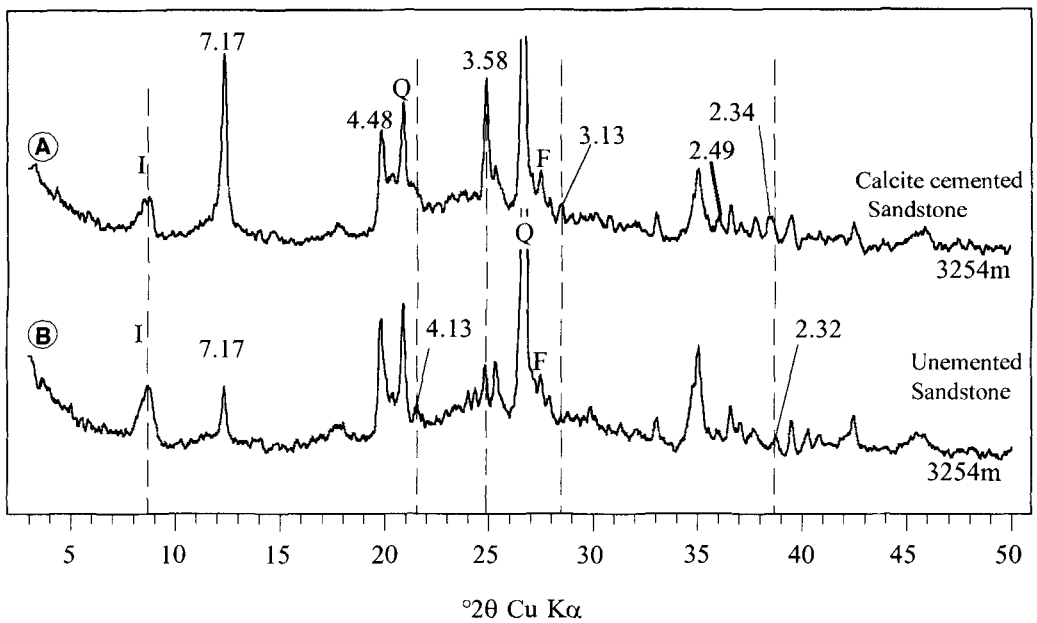

Figure 8. XRD pattern of a powder clay fraction from a calcite cemented sandstone (A) and an uncemented sandstone (B). Peak labels: I = Illite, Q = Quartz, F = Feldspar, D = Dickite, K = Kaolinite.

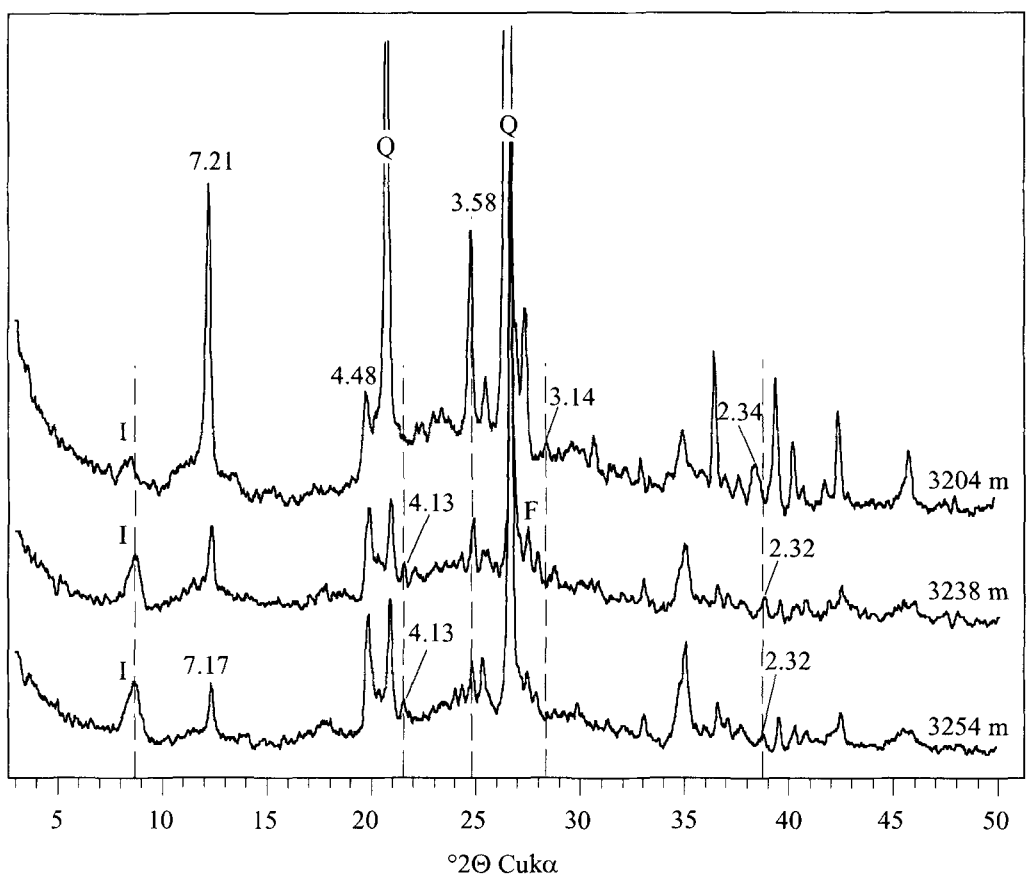

Figure 9. XRD pattern of a random oriented powder clay fraction (<5 μm) of uncemented sandstones showing the evolution of the crystallographic structure of kaolin (polytype) with depth. Peak labels: I = Illite, F = Feldspar, Q = Quartz.

https://doi.org/10.1346/CCMN.1999.0470303 Published online by Cambridge University Press

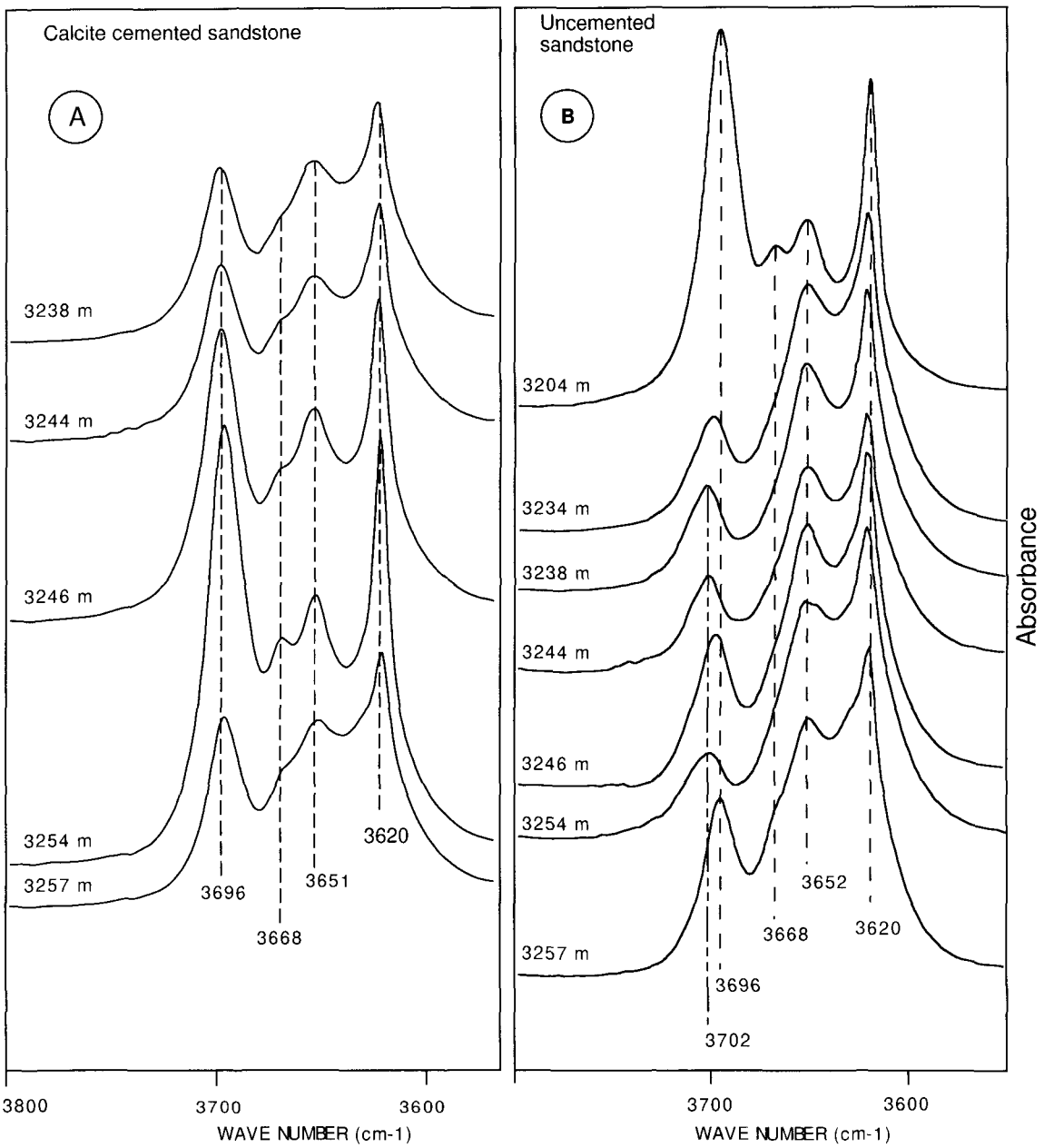

Figure 10. IR spectra of clay fractions (<5 μm) from a calcite-cemented sandstone (A) and an uncemented sandstone (B). The four characteristic bands of kaolinite are present in the calcite-cemented sandstone. Only three bands are present in uncemented sandstone from the same depth, characterizing the dickite polytype. The evolution of the IR reflectance spectra as a function of depth in the uncemented sandstone is shown in B whereas in calcite cemented sandstones (A) there is no change with depth.

Lanson *et al.*, 1996; Lanson and Besson, 1992). However, comparison of samples from different depths shows variations of the relative intensity of each gaussian curve (Figures 11 and 12). PCI (poorly crystallized illite) is more intense in the deepest samples whereas WCI (well crystallized illite) decreases and "IS" (= ordered mixed layers) presents the same intensity (Table 3).

Relation to illite morphology. XRD patterns of the clay fraction of samples with filamentous and lath illite particles (3204–3260 m depth) have asymmetrical 10 Å reflections. XRD patterns of samples below 3260 m with illite crystals having a platelet morphology display a double peak reflection at 10 and 10.5 Å. The 10.5-Å peak is less intense (Figure 11) or absent on the XRD pattern of the samples showing illite with

https://doi.org/10.1346/CCMN.1999.0470303 Published online by Cambridge University Press

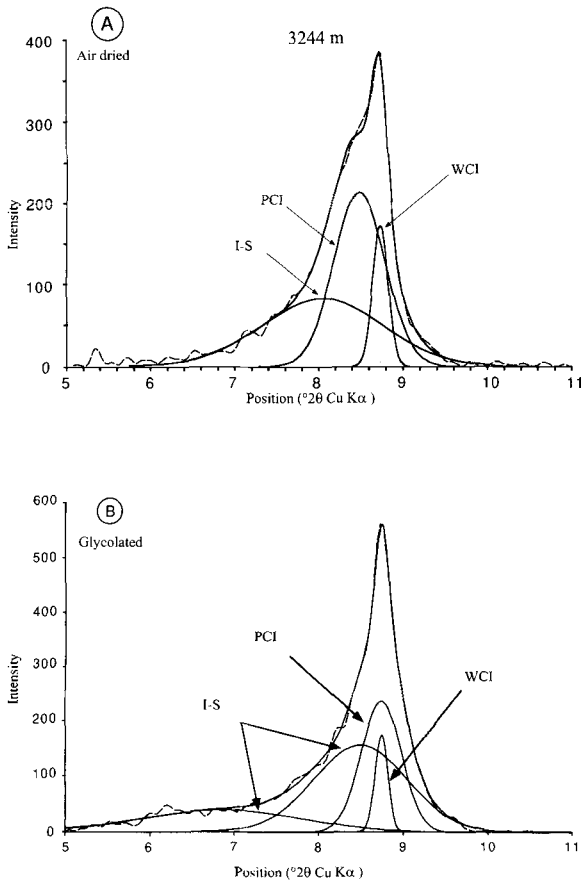

Figure 11. Decomposition of both (A) air-dried and (B) glycolated XRD profile of a sample from 3244 m. Symbols: WCI = Well crystallized illite, PCI = Poorly crystallized illite, "IS" = Ordered mixed layers.

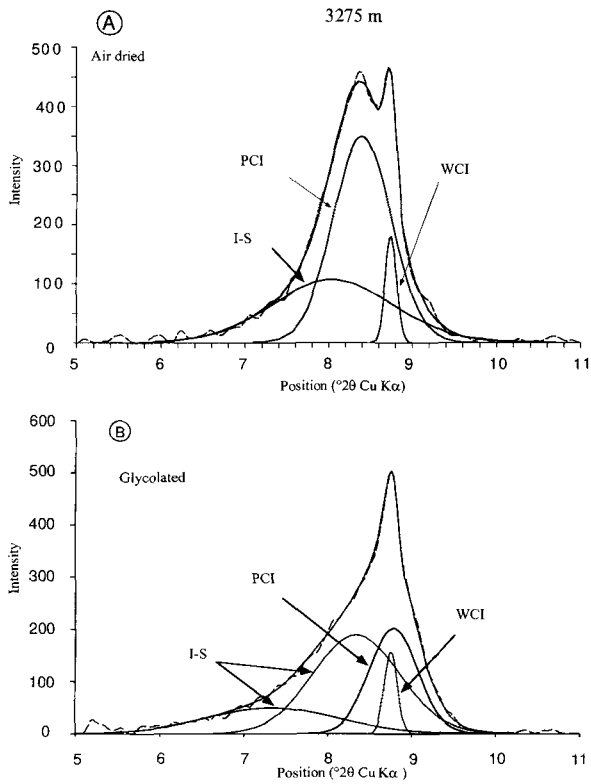

Figure 12. Decomposition of both (A) air-dried and (B) glycolated XRD profile of a sample from 3275 m. Symbols: WCI = Well crystallized illite, PCI = Poorly crystallized illite, "IS" = Ordered mixed layers.

filamentous and lath morphologies. However this peak is more intense in the deeper samples where only platelet illite crystals are present (Figure 12).

DISCUSSION

Chronology of diagenetic processes

According to the petrographical data the chronology of the main diagenetic stages is the following (Figure 13): (1) K-feldspar overgrowths and kaolinite precipitation. Both minerals are enclosed in calcite and therefore formed prior to calcite cementation. (2) Heterogeneous calcite cementation. The calcite cementation is an early diagenetic process which occurred at depths shallower than 1000 m (Potdevin and Hassouta, 1997). (3) Kaolinite-dickite transition. This transition is only visible in uncemented sandstones and therefore occurred after cementation. (4) Illite precipitation, quartz overgrowth, and feldspar dissolution. Illite replaces kaolin in samples below 3204 m. In the deepest sandstones, kaolin is completely absent, and the pore spaces are filled with diagenetic illite. Quartz overgrowths, illite authigenesis, and feldspar dissolution are very rare in the cemented sandstones and therefore occurred after calcite cementation.

Kaolinite precipitation

Petrographic investigations suggest that kaolinite precipitated early in the burial history of these sandstones. Kaolinite precipitation is a major diagenetic

Table 3. Relative intensity of each gaussian curve obtained by decomposition of air-dried XRD pattern between 5–11 °2θ, PCI is more intense in the deepest samples whereas WCI decreases and "IS" presents the same intensity.

Depth (m)	PCI (11 Å)	"IS" (10.51 Å)	WCI (10 Å)
3238 nc	13.01	53.77	33.22
3238.2 nc	21.05	48.42	30.52
3244 nc	13.71	50.47	35.82
3254 nc	16.00	45.07	38.93
3270.3 nc	19.94	64.65	15.48
3272 nc	6.20	55.43	38.37
3274.8 nc	18.21	68.99	12.80
3275 nc	17.03	55.16	27.81

WCI = Well crystallized illite, PCI = Poorly crystallized illite, "IS" = Ordered mixed layers, nc = uncemented sandstone, c = cemented sandstone.

https://doi.org/10.1346/CCMN.1999.0470303 Published online by Cambridge University Press

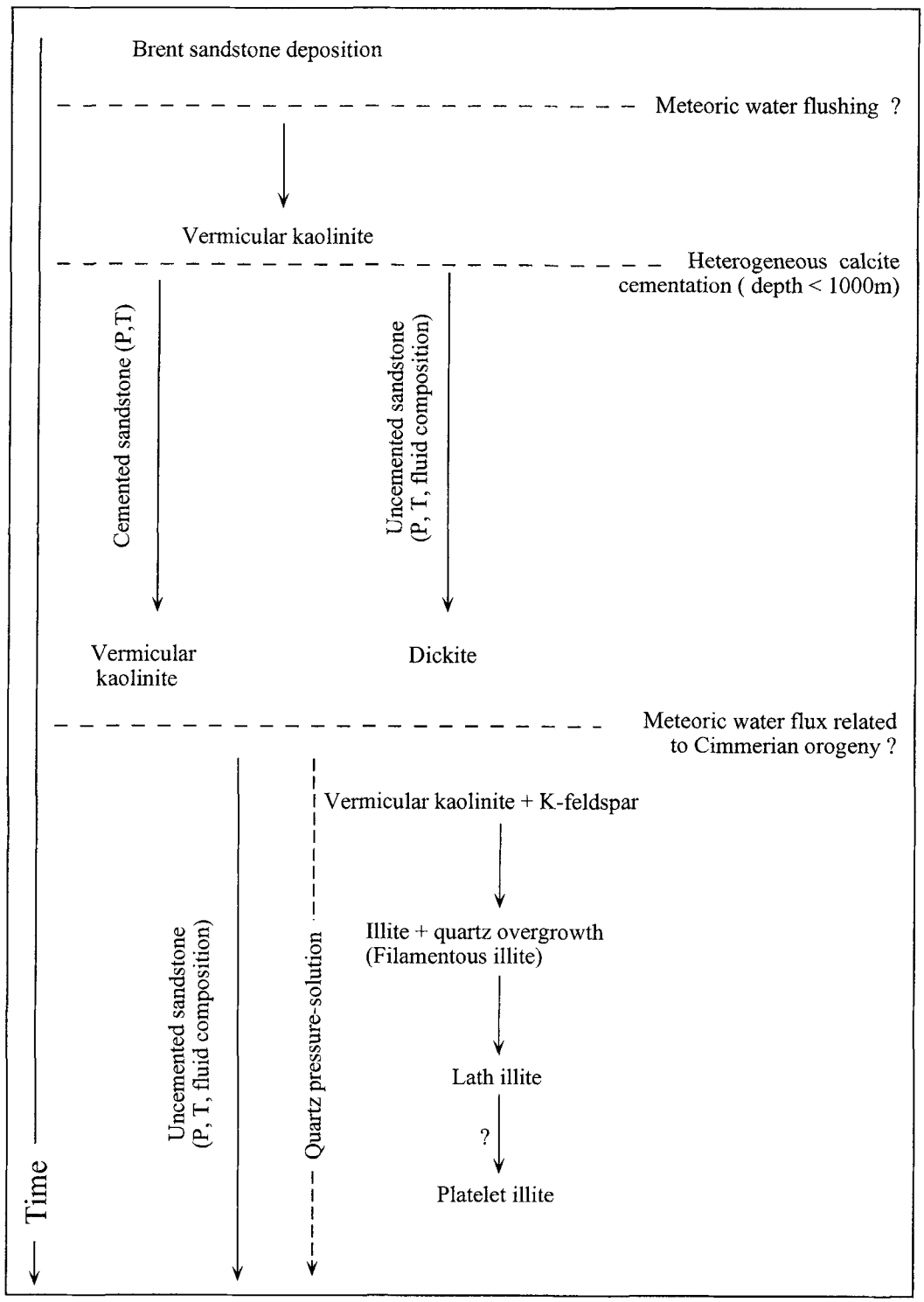

Figure 13. Relationships between the clay diagenetic evolution of the sandstones and the major diagenetic events occurring in the North Sea.

https://doi.org/10.1346/CCMN.1999.0470303 Published online by Cambridge University Press

event in North Sea sandstones and was discussed by several authors. Sommer (1978) and Blanche and Whitaker (1978) suggested that kaolinite precipitated during the later stages of burial diagenesis, whereas an early origin from the precipitation by meteoritic fluids is suggested by other authors (Glasmann, 1992; Bjørlykke and Aagaard, 1992; Haszeldine *et al.*, 1992). The present study confirms the latter hypothesis. Indeed, in the studied sandstones, kaolinite is embedded in a calcitic cement which precipitated at <1000 m depth (Potdevin and Hassouta, 1997).

Calcite cementation

Calcite cementation is an important factor limiting the diagenetic reactions (Kantorowicz *et al.*, 1987; Saigal and Bjørlykke, 1987; Walderhaug *et al.*, 1989). According to Bjørlykke *et al.*, (1992), the carbonate cement intervals in the Brent Group are generally thin, usually <1 m, and usually more abundant in the marine part of the Brent Group (*i.e.*, Rannoch, Etive) than in the deltaic environment of the Ness Formation. This is well demonstrated in studies of the Heather Field (Glasmann *et al.*, 1989). Scotchman *et al.* (1989) showed that in the NW Hutton Field, the sub-littoral sheet sand and the wave-dominated delta-front sand contain more carbonate cement than distributary mouth bar and crevasse splay lobe facies. In the Ellon Field, no relationships are observed between the amount of carbonate cement and the depositional facies. According to Potdevin and Hassouta (1997), the cement fills 34–42% of the sandstone volume, suggesting a porosity before cementation of 37–44% (present porosity in cemented sandstones is ~2–3%, see Table 1). These high-porosity values indicate that calcite cementation is an early diagenetic episode occurring at shallow depth (<1000 m) (Zieglar and Spotts, 1978).

The absence of carbonate fossils in the studied sandstones and the presence of pyrite inclusions inside calcite crystals indicate that the supply of CO_2 could result from organic matter degradation. A similar explanation is given by Walderhaug and Bjørkum (1992) for the calcite origin of the Oseberg Formation. Calcium might be derived from plagioclase, potassium feldspar, and/or heavy minerals dissolution.

Kaolinite-dickite transformation

Changes in the kaolin polytype morphology in sedimentary basins were initially described for a coal basin in Russia (Kossovskaya and Shutov, 1963; Shutov *et al.*, 1970), and more recently in many reservoir sandstones from the North Sea. Ehrenberg *et al.* (1993) described a transition from vermicular to blocky kaolin crystals in Triassic and Jurassic reservoirs of the Norway platform. The same morphological changes were described by McAulay *et al.* (1993) in Brent sandstones from the Hutton and NW Hutton Field (North Sea) and by Lanson *et al.* (1996) in the sandstone reservoirs from the Rotliegend Formation (North Sea). The transition from vermiform to blocky crystals of kaolin is also observed in the present study, but only in uncemented sandstones. IR and XRD data confirm the structural modifications, *i.e.*, the polytype is dependent on the morphological changes. The kaolinite-dickite transition is observed in uncemented sandstone at 3240 m and is characterized by the progressive replacement of vermiform kaolinite by blocky dickite crystals (Figure 14). The depth of the transition is similar to the depth interval (2.8–3.6 km) proposed by Ehrenberg *et al.* (1993) and Beaufort *et al.* (1998) in the sandstone reservoirs from the continental platform of Norway and from the Rotliegend Formation, respectively. Ehrenberg *et al.* (1993) suggested that the kaolinite-dickite transition is temperature dependant and that it occurs at ~120°C.

The morphological changes observed suggest that the kaolinite-dickite transition is a dissolution-precipitation mechanism. However, Lanson *et al.* (1996) suggested that this could be a two step process, consisting of a solid-state transformation without any morphological changes, followed by a dissolution-precipitation reaction involving replacement of vermiform kaolin by blocky crystals. Further work is needed to confirm this hypothesis.

Diagenetic illite

SEM observations of the sandstones above 3260 m show the presence of filamentous and lath particles of illite. These particles seem to grow from kaolinite layers, suggesting that an alteration of kaolinite into illite occurred in these sandstones. Illite authigenesis coinciding with kaolinite and K-feldspar dissolution was described previously in the Brent sandstones from the North Sea by several authors (Bjørlykke, 1983; Bjørkum *et al.*, 1993; Bjørlykke and Aagaard, 1992). The reaction which results in the formation of illite is expressed as (Bjørlykke, 1983):

$$Al_2Si_2O_5(OH)_4 + 0.75KAlSi_3O_8 \rightarrow K_{0.75}Al_2(Si_{3.25}Al_{0.75}O_{10})(OH)_2 + SiO_2 + H_2O$$

Kaolinite + K-Feldspar → Illite + Quartz

A similar reaction can be proposed in the uncemented sandstones. For instance, in thin sections, K-feldspar dissolution coincides with the appearance of filamentous illite. To characterize and quantify the mobility of elements during illite precipitation in the studied sandstones, mass-balance calculations by the Gresens method (Potdevin, 1993) were performed, comparing the chemical composition of cemented and uncemented sandstones (Potdevin and Hassouta, 1997). Gluyas and Coleman (1992) performed a similar com-

https://doi.org/10.1346/CCMN.1999.0470303 Published online by Cambridge University Press

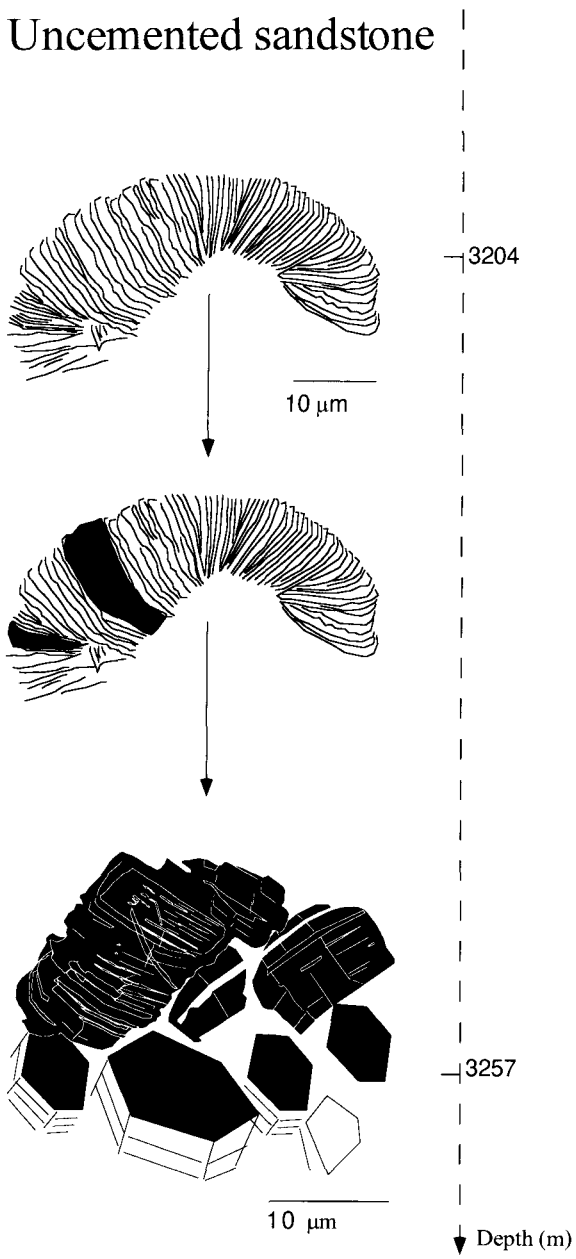

Figure 14. Schematic diagram of kaolin-morphology changes with depth in the uncemented sandstones.

parison in about ten reservoir sandstones, of Permian to Tertiary ages, from oilfields worldwide. They show that some early carbonate concretions preserve both the sedimentary fabric and the composition of the sandstones before calcite cementation from later diagenetic processes. In our case, the cemented sandstone represents the sandstones before illite authigenesis and the uncemented sandstone containing illite represents the final stage of the rock after illite precipitation. Composition-volume diagrams following Gresens (1967) show that Si, Al, and K among other elements are immobile during diagenesis (Potdevin and Hassouta, 1997; Figure 15). Therefore, these elements are not brought by fluid flow and illite precipitation occurred in a system closed to Si, Al, and K. The K of illite is provided by dissolution of K-feldspar and the silica released by kaolinite and feldspar dissolution results in quartz overgrowths. In the studied uncemented sandstones, both mass-balance computations and observations agree with the reaction proposed by Bjørlykke (1983) to explain illite authigenesis.

Below 3260 m, illite with a platelet morphology is the only clay mineral present in the pore spaces of the uncemented sandstones. The morphological changes of illite particles with depth could be related to an increase in the crystallinity with burial. However, below 3260 m, clays are in smaller proportion according to modal analyses and kaolinite is absent. Platelet illite crystals seem to have a different origin; they could have precipitated directly from fluids without a kaolin precursor. Greenwood *et al.* (1994) described similar diagenetic phases in the sandstones sampled in the Hingin Formation from the Brae in the North Sea. These authors suggested that diagenetic kaolin was probably inhibited by temperature and depth of burial. Furthermore, the decomposition of the XRD patterns between 5–11 °2θ suggests a decrease in illite crystallinity, *i.e.*, an increase of the PCI (10.5 Å) curve *vs.* the WCI (10 Å) with depth. The increase of the 10.5-Å reflection is correlated with the presence of platelet illite, whereas above 3260 m, where illite particles present a filamentous or lath morphology, the 10-Å reflection is more intense. Filamentous and lath morphologies are found at depth lower than 3260 m in the shoreface facies where detrital micas are very abundant. Therefore, the contribution of the diagenetic illite (10.5-Å peak) could be masked by the stronger contribution of the detrital mica (10-Å peak) within the clay fraction. In the deeper samples (>3260 m) the sedimentary facies changes (tidal complex), detrital micas are less abundant, and the diagenetic illite reflection becomes relatively more intense. The second explanation for the increase of the 10.5-Å reflection in the deeper samples is that platelet particles could correspond to poorly crystallized illite that directly precipitated from fluids.

Factors promoting clay diagenesis in sandstone reservoirs

The clay diagenetic evolution described is clearly different in cemented and uncemented sandstones (Figure 13). Mineralogical data (IR, XRD, and SEM) suggest that kaolinite is the unique authigenic clay mineral in all the studied cemented sandstones whereas a kaolinite-dickite transition is observed in the uncemented sandstones with increasing depth.

https://doi.org/10.1346/CCMN.1999.0470303 Published online by Cambridge University Press

A

Sample	3238 c	3238 nc
SiO2	47.20	79.00
Al2O3	5.40	8.80
Fe2O3	1.30	1.20
MnO	0.07	0.01
MgO	0.88	0.19
TiO2	0.62	0.80
CaO	22.90	0.20
Na2O	0.45	0.59
K2O	1.48	2.40
S	0.80	1.14
LOI	18.61	4.77
Total	99.71	99.10
Density	2.615	2.025

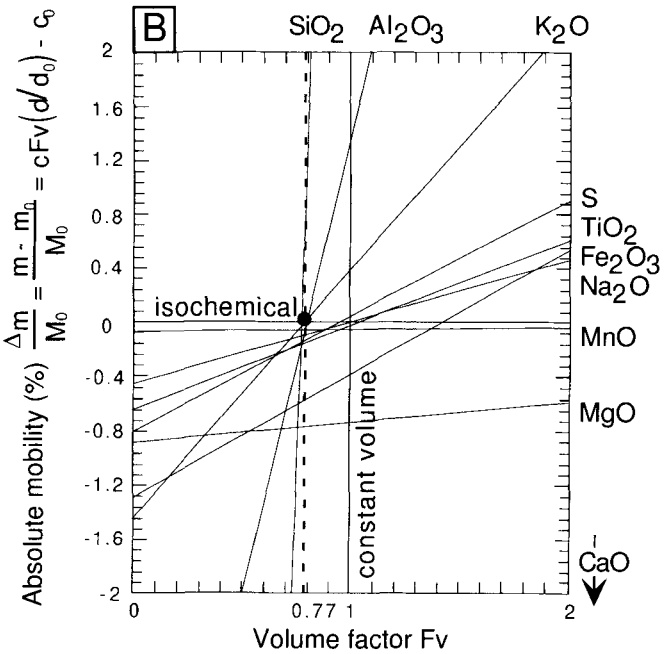

Figure 15. An example of mass-balance calculations of illite authigenesis and quartz overgrowths using the Gresens method (1967). (A) The chemical analysis of the calcite cemented sandstone (sample 3238 c) gives the rock composition before illite authigenesis and quartz overgrowths. The chemical analysis of an uncemented sandstone sampled from the same lithology (3238 nc) gives the rock composition after illite authigenesis and quartz overgrowths. (B) Composition-volume diagram of absolute mobility of major oxides $\Delta m/M_0$ *vs.* Fv. $\Delta m/M_0$ the gain or loss of an oxide (in mass percentage of initial rock) is given by the general relation derived by Gresens (1967). In this diagram, the absolute mobilities of the oxides are graphically shown *vs.* the possible volume changes accompanying the transformation from a cemented sandstones to an uncemented one. Symbols m_0 and m are the mass of the oxide in the initial and final rock (*i.e.*, the cemented and uncemented sandstones), c_0 and c are the weight percentages in this oxide, d_0 and d the densities and Fv the volume factor or ratio of final volume to initial volume. In the composition-volume diagram, the three major elements Si, Al, and K are simultaneously immobile for a Fv value of 0.77 (*i.e.*, a volume change of 23%). It cannot be a coincidence (Gresens, 1967) and these elements are really immobile during illite authigenesis and quartz overgrowths. CaO, MgO, MnO, and FeO mobilities are related to carbonate cementation (see Potdevin and Hassouta, 1997 for a more comprehensive study of mass balance calculations).

These data suggest that the kaolinite-dickite transition can be inhibited by the calcite cement and that temperature and burial are not the only parameters controlling this transition. Zimmerle and Rösch (1991) suggested that the dickite occurrence could be restricted to sedimentary rocks of high porosity and permeability. This is also confirmed in the present study: in cemented sandstones (0–3% porosity) kaolinite is the only kaolin phase formed before calcite cementation and in uncemented sandstones (13–20% porosity) both kaolinite and dickite were identified. By comparison, Ehrenberg *et al.* (1993), McAulay *et al.* (1993), and McAulay *et al.* (1994) indicated that temperature is the major factor controlling the kaolinite-dickite transition. A recent study by Buatier *et al.* (1997) of clay-mineral evolution in thrust faults from the south Pyrenean basin demonstrated that deformation could be an important factor promoting dickite crystallization. The present study demonstrates that porosity and permeability are important parameters also. The calcite cement would prevent fluid flow in cemented sandstones. By filling the pores, calcite cement will prevent fluid-rock interactions and chemical reactions by dissolution-precipitation, such as the kaolinite-dickite transition.

CONCLUSIONS

The sandstones of the Ellon Field reservoir (North Sea) show a complex diagenetic evolution; the first authigenic clay mineral is kaolinite which precipitated during early diagenesis. Then, the sandstones were heterogeneously cemented by calcite. This calcite cement preserved kaolinite, whereas in uncemented sandstones, kaolinite was progressively replaced by dickite with increasing depth. Later, illite precipitated in uncemented sandstones. Its morphology changes with depth: filamentous, lath, and platelet illites are successively found at 3204, 3244, and 3275 m. This study shows that temperature and depth are not the only parameters which control clay reactions (kaolinite-dickite transition, illite precipitation). Pore space availability, fluid composition, or fluid flow could be also important factors. Our data suggest that the kao-

https://doi.org/10.1346/CCMN.1999.0470303 Published online by Cambridge University Press

linite-dickite transition cannot be used as a simple geothermometer.

ACKNOWLEDGMENTS

We are indebted to S.N. Erhenberg and M. Batchelder for their constructive review of the manuscript and to TOTAL-CST France for permission to release this study. C. Demars and F. Sommer (TOTAL-CST) are acknowledged for providing the samples studied and S. Petit (University of Poitiers) for helping us with the IR spectra study. The comments and discussions with E. Brosse, C. Durand (IFP), and B. Lanson (University of Grenoble) were also greatly appreciated.

REFERENCES

Beaufort, D., Cassagnabere, A., Petit, S., Lanson, B., Berger, G., Lacharpagne, J.C., and Johansen, H. (1998) Kaolinite-to-dickite reaction in sandstone reservoirs. *Clay Minerals*, **33,** 297–316.

Bjørkum, P.A., Walderhaug, O., and Aase, N.E. (1993) A model for the effect of illitization on porosity and quartz cementation of sandstones. *Journal of Sedimentary Petrology*, **63,** 1089–1091.

Bjørlykke, K. (1983) Diagenetic reaction in sandstones. In *Sediment Diagenesis, NATO*, A. Parker and B.W. Sellwood, eds., Advanced Study Institute Series, Reidel Publishing Company, Boston, 169–213.

Bjørlykke, K. and Aagaard, P. (1992) Clay Minerals in North Sea Sandstones. In *Origin, Diagenesis, and Petrophysics of Clay Minerals in Sandstones*, D.W. Houseknecht and E.D. Pittman, eds., Society of Economic Paleontologists and Mineralogists Special Publication, **47,** 65–80.

Bjørlykke, K., Nedkvite, T., Ramm, M. and Saigal, G.C. (1992) Diagenetic processes in Brent Group (Middle Jurassic) reservoirs of the North Sea: An overview. In *Geology of the Brent Group*, A.C. Morton, R.S. Haszeldine, M.R. Giles, and S. Brown, eds., Geological Society (London) Special Publication, **61,** 263–287.

Blanche, J.B. and Whitaker J.H.Mc D. (1978) Diagenesis of part of the Brent Sand Formation (Middle Jurassic) of the northern North Sea Basin. *Journal of the Geological Society (London)*, **135,** 73–82.

Bowen, J.M. (1975) The Brent Oil Field. In *Petroleum and the Continental Shelf of Northwest Europe*, A.W. Woodland, ed., Applied Science Publishers, London, 353–360.

Buatier, M.D., Travé, A., Labaume, P., and Potdevin, J.L. (1997) Dickite related to fluid-sediment interaction and deformation in pyrenean thrust-fault zones. *European Journal of Mineralogy*, **9,** 875–888.

Deegan, C.E. and Scull, B.J. (1977) A standard lithostratigraphic nomenclature for the central and northern North Sea. Report of the Institute of Geological Sciences, **77/25**.

Ehrenberg, S.N. Aagaard, P., Wilson, M.J., Fraser, A.R., and Duthie, D.M.L. (1993) Depth-dependent transformation of kaolinite to dickite in sandstones of the Norwegian continental shelf. *Clay Minerals*, **28,** 325–352.

Faure, J.L. (1990) Failles normales, coupes équilibrées et subsidence dans les bassins en extention. Ph.D. thesis, Université de Montpellier, Montpellier, France, 256 pp.

Giles, M.R., Stevenson, S., Martin, S., Cannon, S.J.C., Hamiliton, P.J., Marshall, J.D., and Samways, G.M. (1992) The reservoir properties and diagenesis of the Brent group: A regional perspective. In *Geology of the Brent Group*, A.C. Morten, R.S. Haszeldine, M.R. Giles, and S. Brown, eds., Geological Society (London) Special Publication, **61,** 289–327.

Glasmann, J.R. (1992) The fate of feldspar in Brent Group reservoirs, North Sea: A regional synthesis of diagenesis in shallow, intermediate, and deep burial environments. In *Geology of the Brent Group*, A.C. Morton, R.S. Haszeldine, M.R. Giles, and S. Brown, eds., Geological Society (London) Special Publication, **61,** 329–350.

Glasmann, J.R., Lundegard, P.D., Clark, R.A., Penny, B.K., and Collins, I.D. (1989) Geochemical evidence for the history of diagenesis and fluid migration: Brent sandstone, Heather Field, North Sea. *Clay Minerals*, **24,** 255–284.

Gluyas, J. and Coleman, M. (1992) Material flux and porosity changes during sediment diagenesis. *Nature*, **365,** 52–54.

Greenwood, P.J., Sha, H.F., and Fallick, A.E. (1994) Petrographic and isotopic evidence for diagenetic processes in middle Jurassic sandstone and mudrocks from the Brea, North Sea. *Clay Minerals*, **29,** 637–650.

Gresen, R.L. (1967) Composition-volume relationships of metamorphism. *Chemical Geology*, **2,** 47–55.

Hancock, N.J. and Taylor, A.M. (1978) Clay mineral diagenesis and oil migration in the Middle Jurassic Brent Sand Formation. *Journal of the Geological Society (London)*, **135,** 69–72.

Haszeldine, R.S., Brint, J.F., Fallick, A.E., Hamilton, P.J., and Brown, S. (1992) Open and restricted hydrologies. In *Geology of the Brent Group*, A.C. Morton, R.S. Haszeldine, F.R. Giles, and S. Brown, eds., Geological Society (London) Special Publication, **61,** 401–419.

Jourdan, A., Thomas, M., Brevart, O., Robson, P., Sommer, F., and Sullivan, M. (1987) Diagenesis as the control of the Brent sandstone reservoir properties in the Greater Alwyn area (East Shetland basin). In Petroleum Geology of North West Europe, J. Brooks and K. Gllennie, eds., Graham & Trotman, London, 951–961.

Kantorowicz, J. (1984) The nature, origin and distribution of authigenic clay minerals from Middle Jurassic Ravenscar and Brent Group sandstones. *Clay Minerals*, **19,** 359–375.

Kantorowicz, J.D., Bryant, I.D., and Daans, J.M. (1987) Controls on the geometry and distribution of carbonate cements in Jurassic sandstones: Bridport Sands, southern England and Viking Group, Troll Field, Norway. In *Diagenesis of Sedimentary Sequences*, J.D. Marshall, ed., Geological Society (London) Special Publication, **36,** 102–118.

Kossovskaya, A.G. and Shutov, V.D. (1963) Facies of regional epi-and metagenesis. *International Geology Review*, **7,** 1157–1167.

Lanson, B. and Beson, G. (1992) Characterization of the end of smectite-to-illite transformation: Decomposition of X-ray patterns. *Clays and Clay Minerals*, **40,** 40–52.

Lanson, B., Beaufort, D., Berger, G., Baradat, J., and Lacharpagne, J.C. (1996) Illitization of diagenetic kaolinite-to-dickite conversion series: late-stage diagenesis of the lower Permian Rotliegend sandstone reservoir, Offshore of the Netherlands. *Journal of Sedimentology Research*, **66,** 501–518.

Marshall, D.J. (1998) *Cathodoluminescence of Geological Materials*. Unwin Hyman, Boston, 146 pp.

McAulay, G.E., Burley, S.D., and Johnes, L.H. (1993) Silicate mineral authigenesis in the Hutton and NW Hotton fields: implications for sub-surface porosity development. In *Petroleum Geology of Northwest Europe*, J.R. Parker, ed., Geological Society, London, 1337–1392.

McAulay, G.E., Burley, S.D., Fallick, A.E., and Kusznir, N.J. (1994) Palaeohydrodynamic fluid flow regimes during diagenesis of the Brent group in the Hutton-NW Hutton reservoirs, constraints from oxygen isotope studies of authigenic kaolin and reverse flexural modelling. *Clay Minerals*, **29,** 609–626.

Potdevin, J.L. (1993) Gresens 92: A simple Macintosh program of the Gresens method. *Computers & Geosciences*, **19,** 1229–1238.

Potdevin, J.L. and Hassouta, L. (1997) Bilan de matière des processus d'illitisation et de surcroissance de quartz dans

un réservoir pétrolier du champ d'Ellon (Zone d'Alwyn, Mer du Nord). *Bulletin de la Societé Géologique de France*, **168,** 219–229.

Reynolds, R.C., Jr. (1985) NEWMOD a computer program for the calculation of one dimensional diffraction patterns of mixed-layered clays. R.C. Reynolds, Jr., 8 Brook Drive, Hanover, New Hampshire.

Saigal, G.C. and Bjørlykke, K. (1987) Carbonate cements in clastic reservoir rocks from offshore Norway-relationships between isotopic composition, textural development and burial depth. In *Diagenesis of Sedimentary Sequences*, J.D. Marshall, ed., Geological Society (London) Special Publication, **36,** 313–324.

Scotchman, I.C., Johnes, L.H. and Miller, R.S. (1989) Clay diagenesis and oil migration in Brent Group sandstones of NW Hutton Field, UK North Sea. *Clay Minerals*, **24,** 339–374.

Shutov, V.D., Aleksanddrova, A.V., and Losievskaya, S.A. (1970) Genetic interpretation of the polymorphism of the kaolinite group in sedimentary rocks. *Sedimentology*, **15,** 69–82.

Sommer, F. (1978) Diagenesis of Jurasic sandstones in the Viking Graben. *Journal of the Geological Society (London)*, **135,** 63–67.

Thomas, M. (1986) Diagenetic sequences and K/Ar dating in sandstones, central Viking Graben: Effects on reservoir properties. *Clay Minerals*, **21,** 375–378.

Walderhaug, O. and Bjørkum, P.A. (1992) Effect of meteroic water flow on calcite cementation in the Middle Jurassic Oseberg Formation, Well 30/3-2, Veslefrikk Field, Norwegian North Sea. *Marine and Petroleum Geology*, **9,** 307–318.

Walderhaug, O., Bjørkum, P.A., and Nordgard Bolas, H.M. (1989) Correlation of calcite cemented layers in shallow marine sandstones of the Fensfjord Formation of the Brage Field. In *Correlation in Hydrocarbon Exploration*, J.D. Collisson, ed., Norwegian Petroleum Society, Graham and Trotman, London, 367–375.

Zieglar, D.L. and Spotts, J.H. (1978) Reservoir and source bed history in the Great Valley, California. *American Association of Petroleum Geologists Bulletin*, **62,** 813–826.

Zimmerle, W. and Rösch, H. (1991) Petrogenetic significance of dickite in European sedimentary rocks. *Zentralblatt für Geology und Paläontologie Teil II: Paläontologie. Stuttgurt* **8,** 1175–1196.

(Received 1 October 1997; accepted 30 September 1998; Ms. 97-092)